SUPPLEMENTAL MATERIAL

Methods of ambient noise tomography

We used seismic data recorded by 30 broadband stations of the YS array (Miller et al., 2016) and three permanent stations (GEOFON Data Center, 1993) in the immediate vicinity (Fig. 1) to produce ambient noise tomographic images of the crust and uppermost mantle. We processed the data by following the procedures described in Bensen et al. (2007) and Porritt et al. (2016). First, we processed the ~4-years' continuous daily vertical-component seismograms by instrument responses correction, removal of the mean and linear trends, and taper processing. They were also down-sampled to one sample per second. We then applied running-average time-domain normalization and spectral whitening to the waveforms. Next, waveforms from all station pairs were cross-correlated and stacked over the entire time period of the deployment. With ~4-years' stacking, surface wave signals from ambient noise cross-correlations appear to be clear and stable. Using the automated frequency-time analysis, we measured Rayleigh wave phase velocity dispersions between periods of 6 s and 37 s from symmetric component of the stacked cross-correlations. At last, we screened the measurements by applying quality control with a minimum signal-to-noise ratio of 4 and a minimum inter-station path length of 1.5 wavelengths in consideration of the far-field assumption of surface wave propagation.

Following Fang et al. (2015), we applied a 3-D direct inversion with all selected dispersions to resolve the shear wave velocities in the crust and uppermost mantle of the Banda Arc region. The algorithm avoids the great-circle propagation assumption by incorporating ray tracing and applies a direct smoothing regularization on the 3-D velocity model. As a result, it considers spatial structural coherence (both horizontal and vertical) and generally works better for dealing with regions of strong structural heterogeneity in comparison to the traditional two-step surface wave tomography (Fang et al., 2015). In the inversion, we used the AK135 (Kennett et al., 1995) model as the starting model and only inverted for the upper 70 km depth. Vp and density were calculated using empirical relationships from Brocher (2005). The grids of the inverting model were set as 0.25° by 0.25° in the horizontal direction and 5 km in the vertical depth direction. The ray paths and sensitivity kernels were updated based on the newly obtained model for each iteration. The weighting parameter that balances data fitting and smoothing regularization term was set as 5 and the damping parameter that stabilizes the LSQR solution was set as 0.1. More details about the method and parameter settings can be found in Fang et al. (2015). The results are shown in Fig. S1.

Using the similar parameter settings, we run a series of checkerboard tests to estimate the model resolution and the robustness of the inversion at different depths. In the test, the true checkers are represented by a perturbation of 4 per cent relative to the AK135 model (Kennett et al., 1995). To build the synthetic datasets, we calculated period-dependent Rayleigh wave travel-times for the same station pairs as in the real data application and added 2 percent random noise. Figure S2 presents the recovered results at six representative depths (15 km, 20 km, 25 km, 30 km, 35 km and 40 km) with checker size of 0.75° by 0.75°. In general, it shows that the shear wave velocity model in the upper 50 km can be robustly resolved in the regions where data coverage is dense.
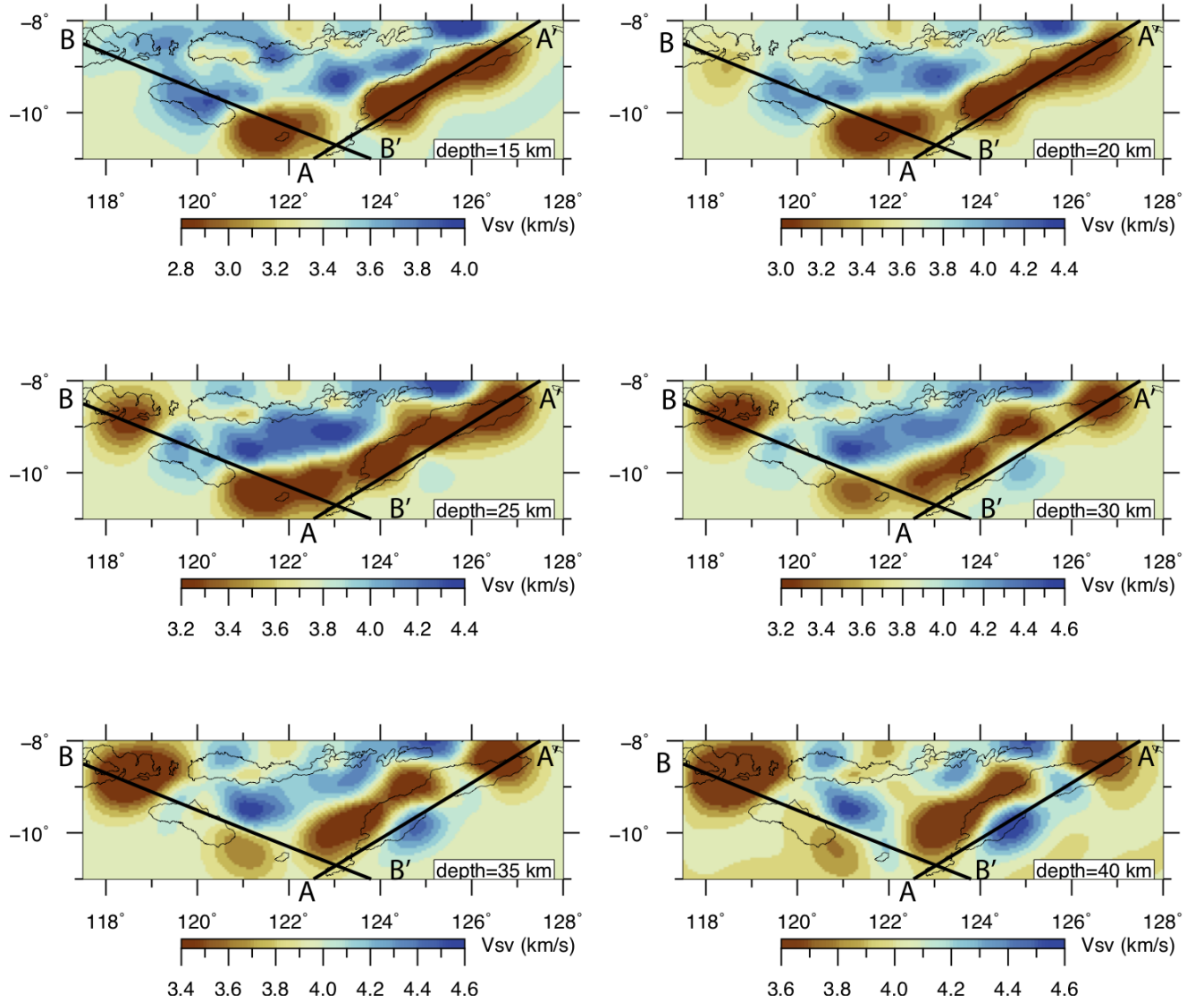
Figure S1. Horizontal slices through the ambient noise based shear wave velocity tomography model at depths indicated in the lower right corner of each panel, which correspond to the same six depths shown in Fig. S2. The black lines indicate the

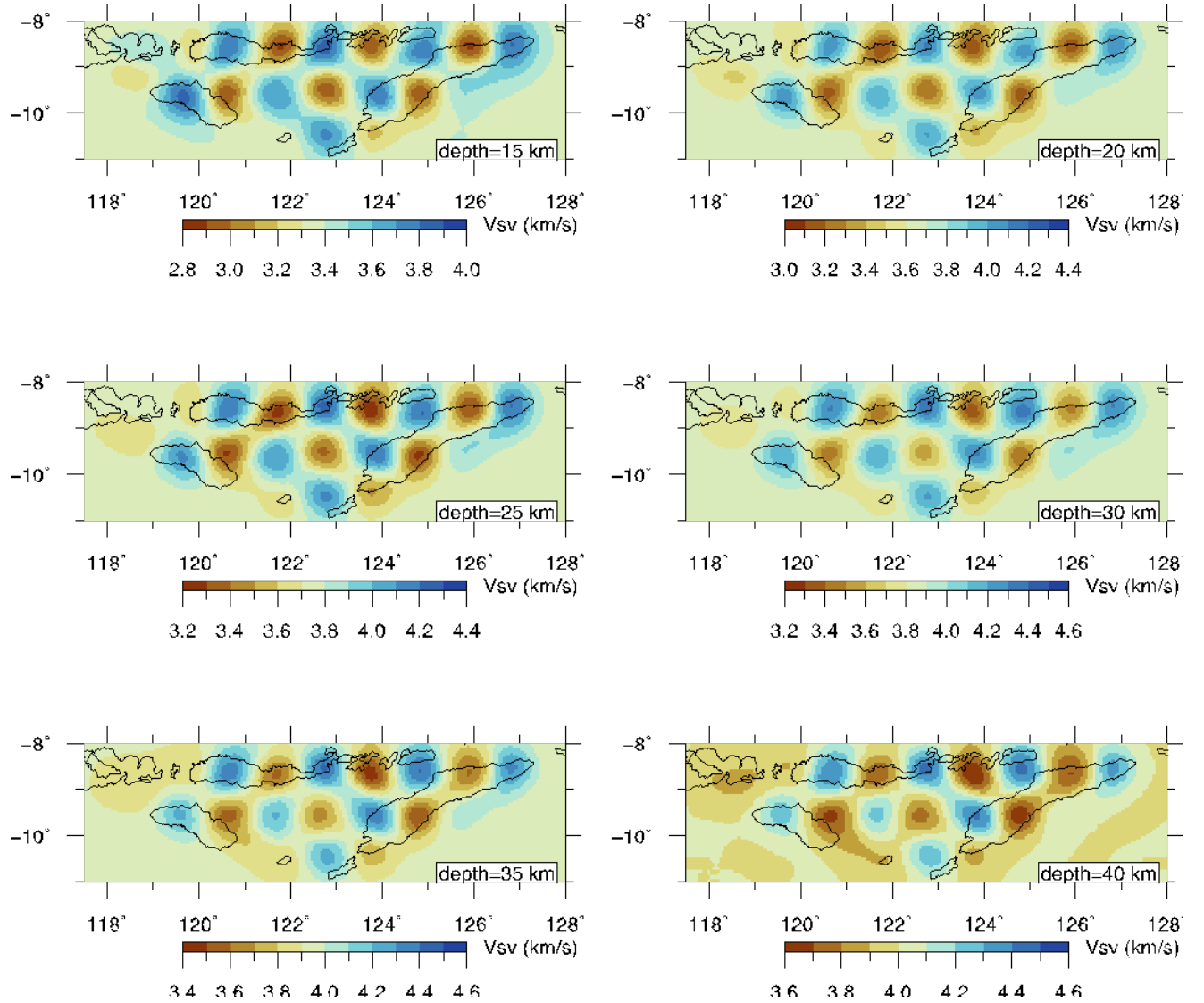*locations of the profiles shown in Fig. 2 in the main text.*

Figure S2. Checkerboard resolution test for the ambient noise tomography at six representative depths maps (same as those in Fig S1).

Methods of river profile inversion

We use the longitudinal topographic profile of rivers to infer the spatial patterns of uplift across the study region, following established inversion approaches and using previously published coastal terrace uplift rates from the Banda region as constraints. The basic principle in the river profile inversion is that a pulse of uplift may manifest as a drop in base level for a river, recorded as a knickzone, or steepened reach, in the river's profile. This knickzone propagates upstream, and by identifying these zones in river profiles, we infer the history of uplift.

In more detail, the evolution of a river profile is controlled by the competition between uplift and erosion, whereby the elevation z at any point along the profile evolves over time t following:

$$\frac{\partial z}{\partial t} = U(x, t) - E(x, t). \tag{1}$$

River long profiles can act as "tectonic tape recorders", preserving the history of tectonic uplift a drainage basin has experienced (Kirby and Whipple, 2001; Pritchard et al., 2009; Roberts and White, 2010). This history can be reconstructed by assuming that river incision is described by the detachment-limited stream power model and that uplift is balanced by erosion. To apply this technique, the erosion term from eq. (1) can be expanded into an advective term, describing knickpoint propagation as a kinematic wave, and a diffusive term, describing the overall lowering of the river profile:

$$\frac{\partial z}{\partial t} = U(t) - v_0 x^m (-\frac{\partial z}{\partial x})^n + \kappa(x)\frac{(\partial^2 z)}{(\partial x^2)} \tag{2}$$

where v_0 is the knickpoint migration velocity if $m = 0$ and $n = 1$, x is the distance downstream from the channel head, κ is the erosional diffusivity, and m and n are positive constants. Diffusive lowering is assumed to be negligible compared to the advective component.

We have used a 1-D river profile inversion technique to determine uplift history for individual river channels (Pritchard et al., 2009). In order to identify the time that any point along a river profile is recording, we use the equation:

$$\tau = -\frac{L^{(1-m)}}{(n-m)v_0} [\frac{1-(x/L)^{1-m/n}}{(x/L)^{m(n-1)/n}}](-\frac{\partial z}{\partial x})^{1-n} \tag{3}$$

where τ is the timing of an uplift rate recorded by the river profile at point x, and L is the total length of the river profile. Calculating $\tau(x)$ allows for calculation of uplift rate if reasonable parameter values are selected, using

$$U(\tau) = v_0 x^m (-\frac{\partial z}{\partial x})^n. \tag{4}$$

For all the rivers in our study area, across Timor, Sumba, Flores, Alor, and Wetar, we assumed $n = 1$, a common assumption in fluvial geomorphology. We used a best-fit value of 0.35 for m on Sumba and 0.43 for the other islands. This allowed us to determine values of v_0 that yielded realistic average uplift rates over the period recorded by these features, using the Matlab *fminsearchbnd* function to fit optimal values independently for each river. We also performed the inversion calculation using a single best-fit value for v_0 across Sumba, but this did not produce uplift histories that fit with independent constraints.

Special criteria to remove non-tectonic influence on river profiles

For all rivers included in profile inversions, we removed downstream segments that appeared to have extensive alluvial fill in the valleys. This is especially apparent for Timor, where many river valleys, especially in the south and east of the island, have wide valley floors consistent with active alluviation. We assume that knickpoints associated with uplift should pass through unconsolidated sediment in alluvial valleys very quickly relative to bedrock, and so consider the points where alluvial valleys begin to be equivalent to base level for studied rivers. We also did not analyze rivers in major karst areas or with large lakes or other sinks. The region of our study area where karst is most topographically important is west Sumba, where internal drainage, sinkholes, and solution valleys are common (Authemayou et al., 2018). As such, we did not analyze rivers in west Sumba. Ira Lalaro is a large lake in extreme eastern Timor which can be seen in the map as a roughly elliptical low-relief area (Fig. S5). We excluded rivers in the Ira Lalaro drainage basin to avoid complications. As a general rule, we tried to minimize analysis of rivers that crossed major active faults (specifically those identified in Duffy et al., 2013) and had major knickpoints that could be associated with major lithologic contrasts. One example of where we removed river segments because of significant lithologic knickpoints is in southeast Sumba and rivers draining the Kananggar Massif igneous basement rocks (Effendi and Apandi, 1981). Another location that required careful selection of rivers for analysis is north central Timor, where Aileu complex metamorphic rocks are thrust over Gondwana sequence sediments (Tate et al., 2014). Where possible, we removed river segments above the lithologic contrast from our analysis but analyzed downstream portions of the network. Figure S7 shows an example river from our analysis that crosses several lithologic contacts. We interpret the two major knickpoints marked with arrows to be reflective of tectonic uplift and that lithology does not exert a strong control on the river profile. This is evidenced by the

lack of a knickpoint at the lowest contact, where young, probably weak synorogenic sediments contact Permo-Triassic rocks upstream without a change in river slope. Similarly, no lithologic knickpoint is found at the contact between the Gondwana Sequence and Banda Terrane rocks moving upstream. We interpret the knickpoint shown at the lower arrow to be created by a change in uplift rate, as the transition into Gondwana Sequence rocks did not produce a knickpoint downstream, where we expect that the rock strength contrast should have been greater. Finally, the upper knickpoint is associated with no major contact or structural feature and is also likely an uplift-driven feature.

Another important problem area is on Flores, where many volcanoes remain active or have been active during the Quaternary. To avoid erroneous interpretation of constructional terrain associated with volcanic activity, we avoided analyzing any rivers with Quaternary volcanoes in their drainage basins. With these precautions, we expect that most remaining knickpoints in the rivers we have analyzed were created by tectonic uplift (Fig. S6).

Inversion results should be interpreted cautiously since basic assumptions inherent to the stream power model are often not met in many rivers (Lague, 2014), and drainage basin reorganization can complicate river histories especially during early topographic evolution of islands (Ramsey et al., 2007). Nonetheless, the broad patterns of reconstructed uplift may yield some general insight into the history of surface deformation, including in the context of uplifting islands (Roberts et al., 2013; Fox et al., 2014). Moreover, in applying the river profile inversion approach to the Banda region, we can take advantage of the widespread and well-dated coral terraces, which provide important independent markers for uplift. On Sumba, an uplifted coral terrace dated to MIS 11 (~400 kyr) is mostly continuous along the west, north, and east coasts of the island (Pirazzoli et al., 1993; Nexer et al., 2015), and on Timor, several terraces have been dated around the island and particularly along the northeastern coast, recording uplift over the past 100-200 ka (Cox, 2009). Overall, the patterns recovered in the river profile analysis are coherent with those observed in the uplifted coral terraces (e.g., Fig. S4), adding some confidence to the interpretation of first-order patterns in reconstructed uplift despite the many associated uncertainties.
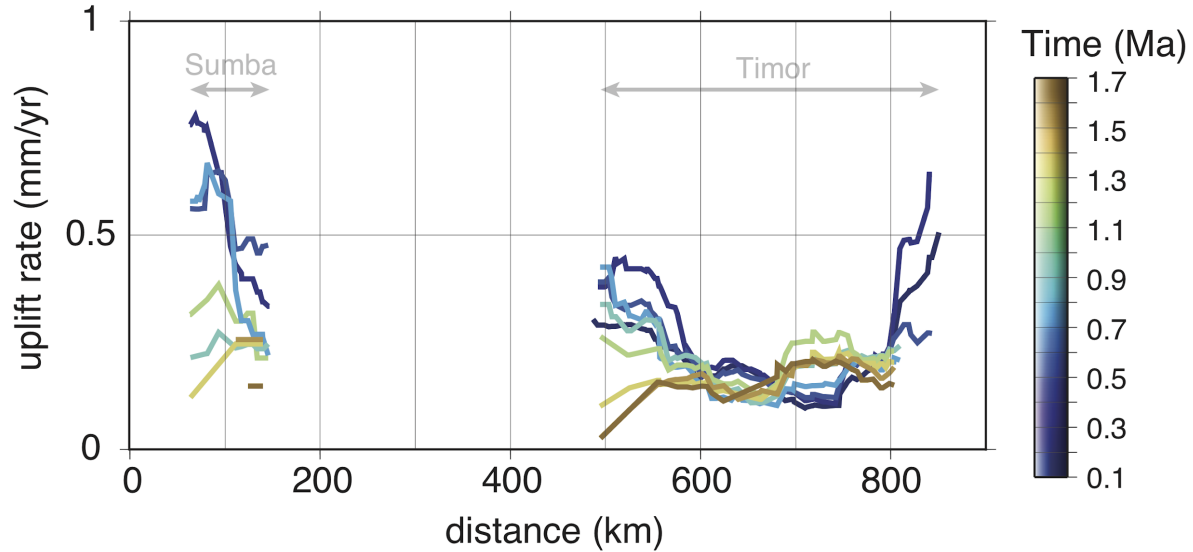
Figure S3. *Profile showing inferred uplift rate reconstructions from river profile inversions across the northern coasts of the outer Banda Arc islands (Sumba and Timor). Independent constraints on uplift rates exist to Marine Isotope Stage 11 (~400 ka) for Sumba, though some uplifted terrace sites in East Timor only record from 100-200 ka. Uplift inversions were along each river in 1D; the profiles shown here are interpolated between river outlets on the north coasts of Sumba and Timor, with the distance measured west to east along a path roughly parallel to the Timor Trough between the islands. Overall, we see a shift from early uplift in the middle of Timor, where topography is highest and uplift was presumably sustained for long periods of time, to more recent accelerated rates at the ends of the island, near the transition between fast and slow velocities imaged in the ambient noise tomography.*
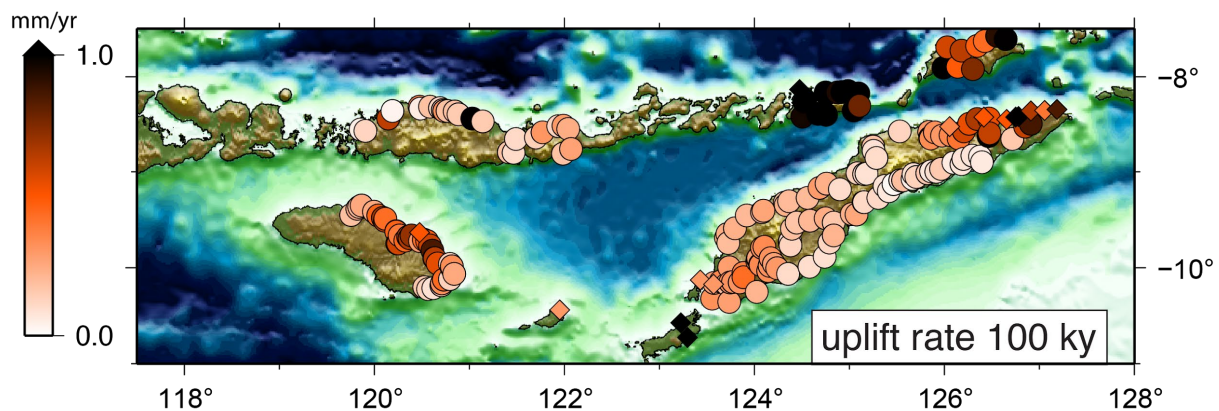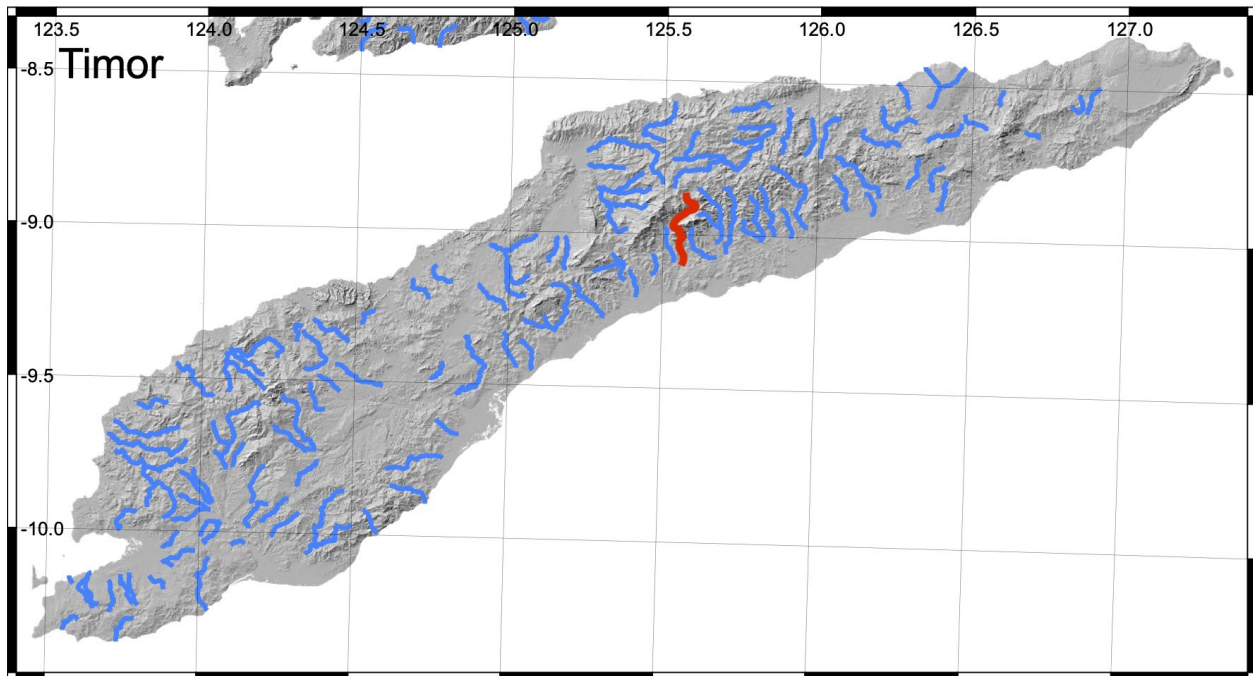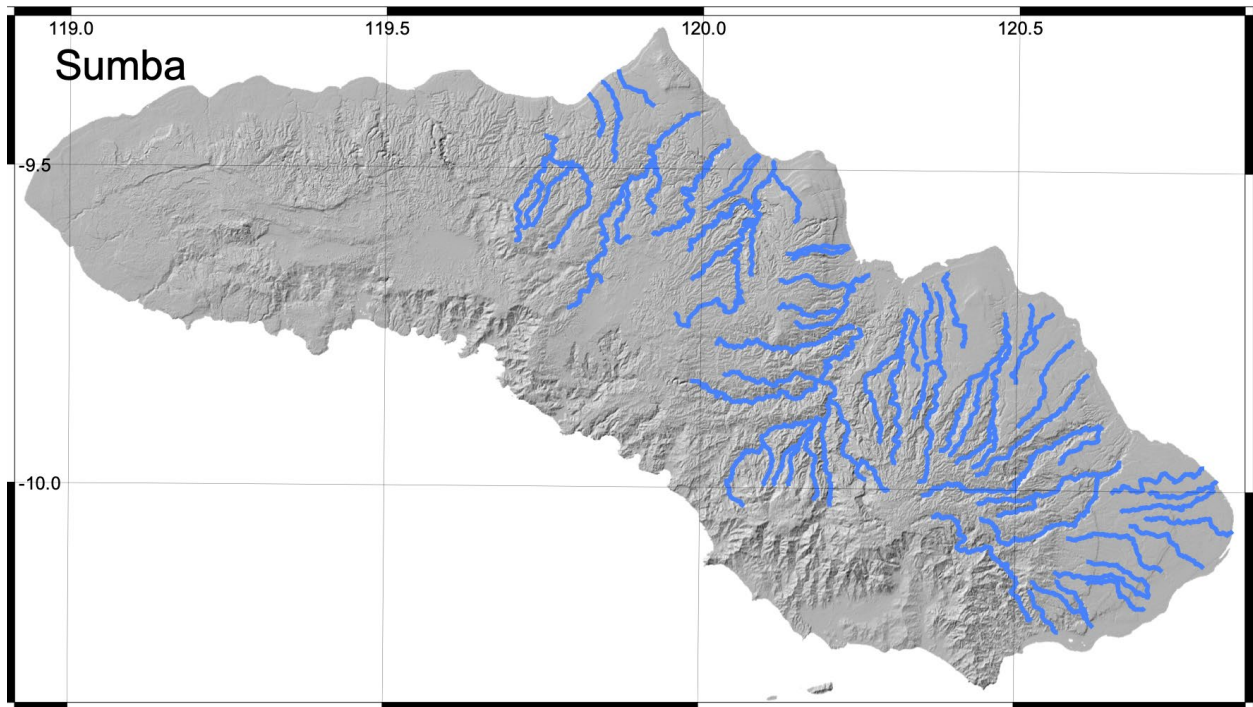

Figure S4. *Uplift rate in mm/year from the past 100 ky, also shown in Fig. 3. Circles are rates inferred for each river profile. Diamonds are coastal terrace uplift rates from published data, also used to constrain the river profile inversions.*
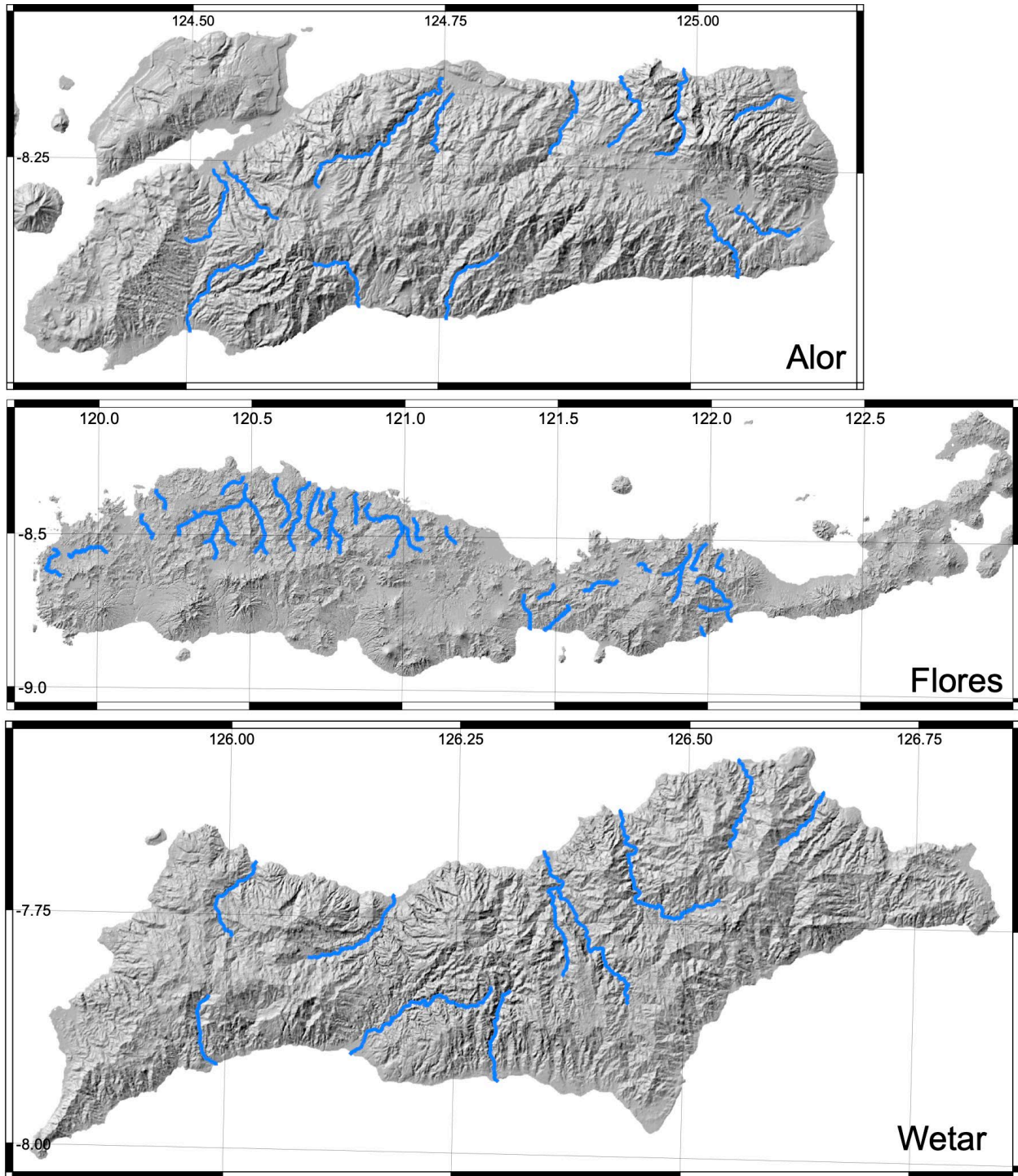
Fig S5. Shaded relief map of all islands included in river profile inversions with analyzed river segments shown in blue. River highlighted in red on Timor is shown in Fig S7.
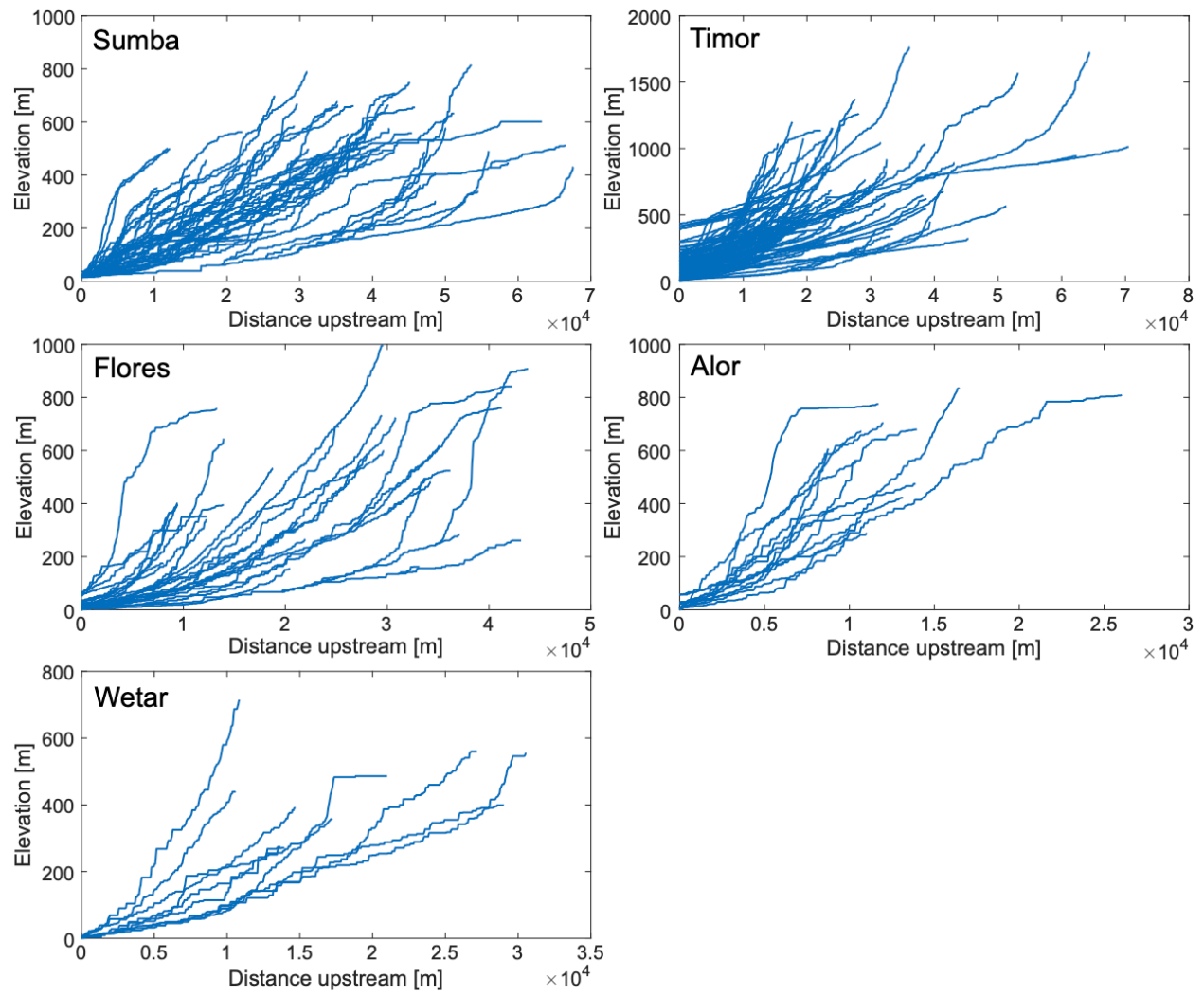
Figure S6. Long profiles of rivers included in inversion analysis for each island as shown in Fig S5.
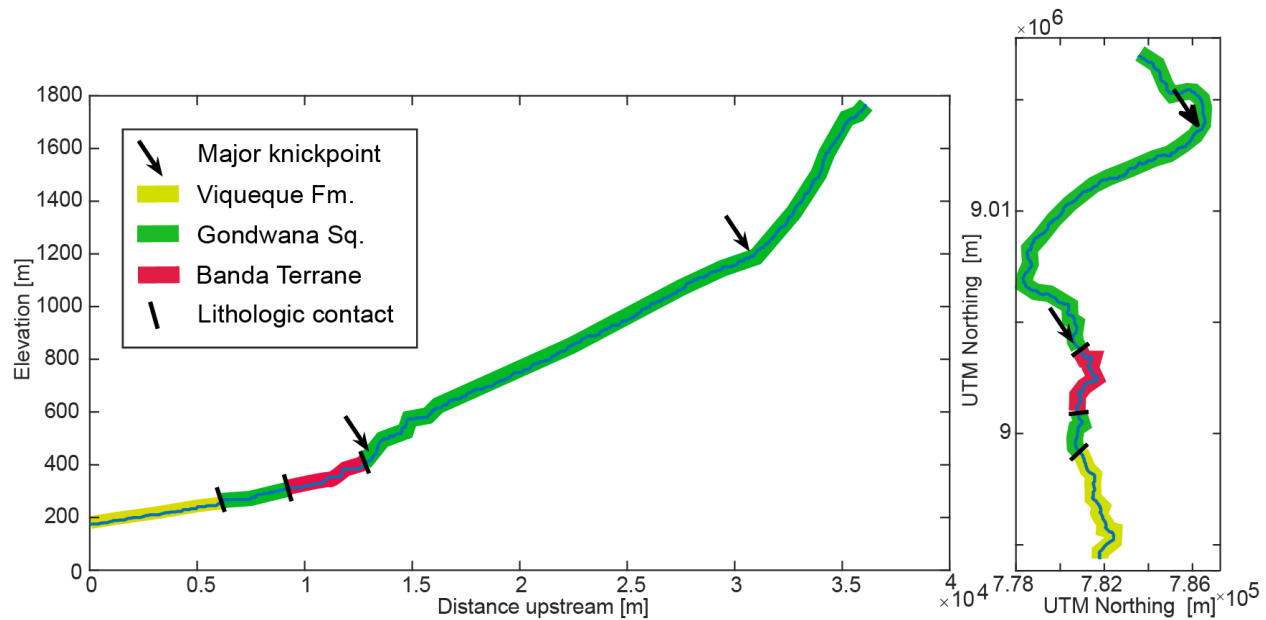
Fig S7. Long profile and map view of river highlighted in red on Fig S5, showing lithologic contacts and major knickpoints. The Viqueque Fm. is a Mio-Pliocene synorogenic unit, the Gondwana Sq. are Permo-Triassic Australian-affinity passive margin sediments, the Banda Terrane is a Cretaceous to Cenozoic metamorphic, volcanic, and carbonate allocthon. Locations of contacts are from Tate et al., (2014).

SUPPLEMENTARY REFERENCES

Authemayou, C., Brocard, G., Delcaillau, B., Molliex, S., Pedoja, K., Husson, L., Aribowo, S., and Cahyarini, S.Y., 2018, Unraveling the roles of asymmetric uplift, normal faulting and groundwater flow to drainage rearrangement in an emerging karstic landscape: Earth Surface Processes and Landforms, v. 43, p. 1885–1898, doi:10.1002/esp.4363.

Brocher, T.M., 2005, Empirical Relations between Elastic Wavespeeds and Density in the Earth's Crust: Bulletin of the Seismological Society of America, v. 95, p. 2081-2092, doi:10.1785/0120050077.

Cox, N. L., 2009, Variable uplift from quaternary folding along the northern coast of East Timor, based on U-series age determinations of coral terraces, 151 pp., Brigham Young University.

Duffy, B., M. Quigley, R. Harris, and U. Ring, 2013, Arc-parallel extrusion of the Timor sector of the Banda arc-continent collision: Tectonics, v. 32, no. 3, p. 641–660, doi:10.1002/tect.20048.

Effendi, A. C. and Apandi, C., 1981, Geological map of Sumba Quadrangle, Nusa Tenggara Unpubl. Map and Report, Geological Research and Development Centre,

Bandung.

Fox, M., Goren, L., May, D.A., and Willett, S.D., 2014, Inversion of fluvial channels for paleorock uplift rates in Taiwan: Journal of Geophysical Research: Earth Surface, v. 119, p. 1853-1875, doi:10.1002/2014jf003196.

GEOFON Data Centre (1993): GEOFON Seismic Network. Deutsches GeoForschungsZentrum 447 GFZ. Other/Seismic Network. doi:10.14470/TR560404.

Kennett, B.L.N., Engdahl, E.R., and Buland, R., 1995, Constraints on seismic velocities in the Earth from travel times: Geophys. J. Int., v. 122, p. 108-124.

Lague, D., 2014, The stream power river incision model: evidence, theory and beyond: Earth Surface Processes and Landforms, v. 39, p. 38-61, doi:10.1002/esp.3462.

Pirazzoli, P.A., Radtke, U., Hantoro, W.S., Jouannic, C., Hoang, C.T., Causse, C., and Borel Best, M., 1993, A one million-year-long sequence of marine terraces on Sumba Island, Indonesia: Marine Geology, v. 109, p. 221–236, doi:10.1016/0025-3227(93)90062-z.

Porritt, R.W., Miller, M.S., O'Driscoll, L.J., Harris, C.W., Roosmawati, N., and da Costa, L.T., 2016, Continent–arc collision in the Banda Arc imaged by ambient noise tomography: Earth and Planetary Science Letters, v. 449, p. 246–258, doi:10.1016/j.epsl.2016.06.011.

Ramsey, L.A., Walker, R.T., and Jackson, J., 2007, Geomorphic constraints on the active tectonics of southern Taiwan: Geophys. J. Int., v. 170, p. 1357-1372, doi:10.1111/j.1365-246X.2007.03444.x.

Roberts, G.G., and White, N., 2010, Estimating uplift rate histories from river profiles using African examples: Journal of Geophysical Research, v. 115, doi:10.1029/2009jb006692.

Tate, G.W., McQuarrie, N., van Hinsbergen, D.J.J., Bakker, R.R., Harris, R., Willett, S., Reiners, P.W., Fellin, M.G., Ganerød, M., and Zachariasse, W.J., 2014, Resolving spatial heterogeneities in exhumation and surface uplift in Timor-Leste: Constraints on deformation processes in young orogens: Tectonics, v. 33, p. 1089-1112, doi:10.1002/2013tc003436.